

ORIGINAL ARTICLE

Topotactically synthesized ultralong LiV_3O_8 nanowire cathode materials for high-rate and long-life rechargeable lithium batteries

Xu Xu^{1,3}, Yan-Zhu Luo^{1,3}, Li-Qiang Mai^{1,2}, Yun-Long Zhao¹, Qin-You An¹, Lin Xu^{1,2}, Fan Hu¹, Lei Zhang¹ and Qing-Jie Zhang¹

High-power applications at fast charge and discharge rates are still significant challenges in the development of rechargeable lithium (Li) batteries. Here, we demonstrate that ultralong LiV_3O_8 nanowire cathode materials synthesized by topotactic Li intercalation are capable of excellent high-rate performance with minimal capacity loss. A specific discharge capacity of 176 mAh g^{-1} can be obtained at the current density of 1500 mA g^{-1} , and the capacity is able to stabilize at 160 mAh g^{-1} after 400 cycles, corresponding to 0.025% capacity fading per cycle. For current density up to 2000 mA g^{-1} , the initial and the six-hundredth cycle capacities can reach 137 and 120 mAh g^{-1} , respectively, corresponding to a capacity fading of only 0.022% per cycle. The ability to provide this level of performance is attributed to a low-charge-transfer resistance, good structural stability, large surface area and suitable degree of crystallinity, and it indicates that LiV_3O_8 nanowires are promising cathode materials for use in high-rate and long-life rechargeable Li batteries.

NPG Asia Materials (2012) 4, e20; doi:10.1038/am.2012.36; published online 22 June 2012

Keywords: high-power; high-rate; lithium batteries; LiV_3O_8 nanowires; topotactic synthesis

INTRODUCTION

With the rapid development of mobile devices and electric vehicles, rechargeable Li batteries are widely considered to be some of the most promising rechargeable batteries.^{1–3} However, the low-power density caused by the low Li ion, and electron transport speed has limited their practical high-power applications. An ideal cathode material for high-rate rechargeable Li batteries should have a high electrical conductivity for fast electron transport, short diffusion distance for fast Li ion migration and a large surface area.⁴ Nanowires can have a tremendous impact in many areas,^{5–10} and for Li batteries, nanowire electrodes have attracted much attention because of their short Li ion diffusion pathway, large electrode–electrolyte contact area and good strain accommodation.^{11–15}

LiV_3O_8 is considered to be an ideal cathode material because of its high-specific capacity, good structural stability, low cost and good safety features. It has been reported that its electrochemical performance is greatly influenced by the morphology and synthesis method.^{16–19} During the past 30 years, many methods have been proposed to improve the electrochemical properties of LiV_3O_8 with different morphologies.^{20–36} However, LiV_3O_8 nanowires with large aspect ratios and surface areas, which are supposed to have a desirable high-rate performance when used as the cathode material in

rechargeable Li batteries, have rarely been reported.²² $\text{H}_2\text{V}_3\text{O}_8$ (reported as $\text{V}_3\text{O}_7 \cdot \text{H}_2\text{O}$; however, from a structural point of view, the formulation $\text{H}_2\text{V}_3\text{O}_8$ is more appropriate than that of $\text{V}_3\text{O}_7 \cdot \text{H}_2\text{O}$ ³⁷) nanowires were reported to have a particularly ultralong one-dimensional morphology and a layered crystal structure similar to LiV_3O_8 ,³⁸ which allow the topotactic Li intercalation to form LiV_3O_8 . This means that the resulting LiV_3O_8 will generally maintain the ultralong morphology and have a large surface area and a short Li ion transport pathway, which are crucial for producing an acceptable high-rate performance. Moreover, the intercalation of settled Li ions in the layers of the LiV_3O_8 structure makes the structure more stable during the charge–discharge process. In the present work, based on the topotactic intercalation mechanism, we proposed a facile and mass-produced route to synthesize ultralong LiV_3O_8 nanowires with excellent high-rate and long-life performance to serve as the cathode material in rechargeable Li batteries.

MATERIALS AND METHODS

Materials

For typical synthesis, V_2O_5 , $\text{LiOH} \cdot \text{H}_2\text{O}$, aniline, alcohol and polyethylene glycol (MW, 4000) were analytical reagent grade and purchased from the

¹State Key Laboratory of Advanced Technology for Materials Synthesis and Processing, WUT-Harvard Joint Nano Key Laboratory, Wuhan University of Technology, Wuhan, China and ²Department of Chemistry and Chemical Biology, Harvard University, Cambridge, MA, USA

³These authors contributed equally to this work.

Correspondence: Professor L-Q Mai, State Key Laboratory of Advanced Technology for Materials Synthesis and Processing, WUT-Harvard Joint Nano Key Laboratory, Wuhan University of Technology, 122 Luoshi Road, Wuhan 430070, China.

E-mail: mlq518@whut.edu.cn or mlq@cmliris.harvard.edu

Received 22 March 2012; revised 7 May 2012; accepted 11 May 2012

Sinopharm Chemical Reagent Co., Ltd (Shanghai, China). All chemicals were used directly without any purification.

Methods

The ultralong LiV₃O₈ nanowires were prepared in two steps. First, the single-crystalline H₂V₃O₈ nanowires were synthesized by a hydrothermal method according to our previous work.³⁸ Second, the obtained H₂V₃O₈ nanowires and LiOH·H₂O (V/Li = 3:1.05) were mixed in alcohol and stirred for 5 h to obtain a homogeneous mixture. Finally, the mixture was heated at 80 °C to allow the alcohol evaporation and then annealed at different temperatures (400 °C, 450 °C and 500 °C) for 10 h to obtain a brown powder.

Characterization

An X-ray diffraction (XRD) measurement was performed to investigate the crystallographic information using a D8 Advance X-ray diffractometer with a non-monochromated Cu K α X-ray source. Field-emission scanning electron microscopy images were collected with a Hitachi S-4800 at an acceleration voltage of 10 kV. Transmission electron microscopy and high-resolution transmission electron microscopy images were recorded with a JEM-2100F STEM/EDS microscope. Brunauer–Emmet–Teller surface areas were measured using a Gemini 2360 instrument to measure the adsorption of nitrogen at –209 °C.

Electrochemical measurement

The electrochemical properties were tested with 2025 coin cells assembled in a glove box filled with pure argon gas. Lithium pellets were used as the anode, 1 M solution of LiPF₆ in ethylene carbon /dimethyl carbonate was used as the electrolyte, and the cathode electrodes were produced with 70% LiV₃O₈ nanowire active material, 20% acetylene black and 10% poly(tetrafluoroethylene). Galvanostatic charge/discharge measurement was performed in the potential range from 4.0 to 1.5 V vs Li/Li⁺ with a multichannel battery testing system (LAND CT2001A). Cyclic voltammetry and AC-impedance spectra were tested with an electrochemical workstation (Autolab PGSTAT 30 and CHI 760D).

RESULTS

Characterization of LiV₃O₈ nanowires

To determine the phase structures of the products, XRD measurements were conducted. The XRD patterns in Figure 1a show that the as prepared LiV₃O₈ nanowires at calcination temperatures of 400 °C, 450 °C and 500 °C (defined as samples 400, 450 and 500, respectively) can all be indexed to a monoclinic structure phase (JCPDS No. 01-072-1193). A small amount of impurity phase Li_{0.3}V₂O₅ was detected, which is attributed to the low reaction temperature. The Li_{0.3}V₂O₅ impurity has also been reported in many other synthesis methods.^{16,19,39,40} Although the samples annealed at different temperatures have consistent peak locations, the peak intensity distributions are different. It has been reported that the crystallinity of LiV₃O₈ increases as the values of I(100)/I(003) and I(100)/I(020) increase.^{41,42} The relative intensity ratios of I(100)/I(003) and I(100)/I(020) calculated from the XRD data are listed in Table 1. It is clear that the crystallinity of the nanowires increases with the calcination temperature.⁴³

Figure 1b shows a scanning electron microscopy image of the precursor H₂V₃O₈ nanowires with a channel structure, which have a diameter of 100–200 nm and a smooth surface. The XRD pattern and transmission electron microscopy image of H₂V₃O₈ nanowires are presented in the Supplementary information (Supplementary Figure S1). Figures 1c–e are the scanning electron microscopy images of samples 400, 450 and 500, respectively. The LiV₃O₈ generally maintained the nanowire morphology of the H₂V₃O₈ precursor, and the length reached hundreds of micrometers (Supplementary Figure S2). The transmission electron microscopy image of sample

450 is shown in Figure 1f, which contains two nanowires with similar diameters. The single-crystal nature of each LiV₃O₈ nanowire was confirmed by selected area electron diffraction analysis in which the diffraction spots matched the [001] lattice direction.

Electrochemical property comparison of LiV₃O₈ nanowires prepared at different calcination temperatures

Cyclic voltammetry results for samples 400, 450 and 500 are shown in Figure 2a. The voltammograms were measured at a sweep rate of 0.1 mV s^{–1} in the potential range from 4.0 to 1.5 V vs Li/Li⁺ at room temperature. It is obvious that sample 450 has a larger curve area and a higher redox peak current than those of samples 400 and 500, suggesting that sample 450 has the highest capacity and the fastest kinetics for Li ion insertion/extraction.^{41,44} Sample 450 is used as an example to explain the electrochemical process. All of these peaks originate from the phase transitions between Li_{1+x}V₃O₈ components with different *x* values (0 < *x* < 3). The peaks at 2.68 V and 2.57 V correspond to Li ion insertion in the empty tetrahedral site to perform a single-phase reaction. It is obvious that the current of these insertion peaks is almost the same as those of the other samples. This phenomenon can be explained as follows: in the initial period, the empty Li ion diffusion paths and tetrahedral sites are convenient for the insertion of Li ions. Then, the further insertion of Li ions into tetrahedral sites leads to a two-phase transition from Li₃V₃O₈ to Li₄V₃O₈ at 2.36 V. The peak at 2.06 V can be attributed to the last step, in which a slower kinetic insertion process occurs as the single-phase transition.¹⁹ The cathodic peaks at 2.5 V and 3.54 V belong to the impurity phase Li_{0.3}V₂O₅.¹⁶ Figure 2b displays the initial charge–discharge curves of LiV₃O₈ nanowire cathodes at the current density of 20 mA g^{–1}. Sample 400 shows the highest discharge capacity of 318 mAh g^{–1}, which may be attributed to the low crystallinity.²⁷ Three discharge plateaus located at ~2.85 V, 2.60 V and 2.20 V can be identified as resulting from the single-phase insertion process, the two-phase transformation from Li₃V₃O₈ to Li₄V₃O₈ and the slower kinetic insertion process, respectively.^{42,45,46} The initial discharge capacities at different current densities are compared (Figure 2c). It can be clearly seen that sample 450 exhibits the highest capacities at the current densities from 50 to 600 mA g^{–1}.

Figures 2d–f are the primary cycling performance comparison of three samples at the current densities of 20, 50 and 100 mA g^{–1}, respectively. At the current density of 20 mA g^{–1}, sample 400 exhibited the best performance during the 20 cycles. At the current density of 50 mA g^{–1}, the initial discharge capacity of samples 400, 450 and 500 were 277, 287 and 283 mAh g^{–1}, respectively. The discharge capacities decreased to 239, 262 and 244 mAh g^{–1} after 50 cycles, corresponding to the capacity retention of 86.05%, 94.63% and 86.21%, respectively. It is obvious that sample 450 exhibited the highest capacity and best cycling performance. The quick capacity decline of sample 400 may result from the low crystallinity, which is unable to support the intercalation and deintercalation process, leading to structure degradation. As a result, some Li ions are bonded to oxygen and cannot be completely extracted, resulting in the loss of capacity.²⁷ Sample 500 also exhibited a lower discharge capacity and a larger capacity loss because of its large size, which increased the energy barrier for Li ion diffusion. The performance at a current density of 100 mA g^{–1} also displayed a similar behavior to that at a current density of 50 mA g^{–1}. Interestingly, during the first several cycles, the capacities decreased rapidly, then recovered cycle by cycle and finally stabilized. It has been reported that at a high current density, the initial capacity fading can be attributed to active

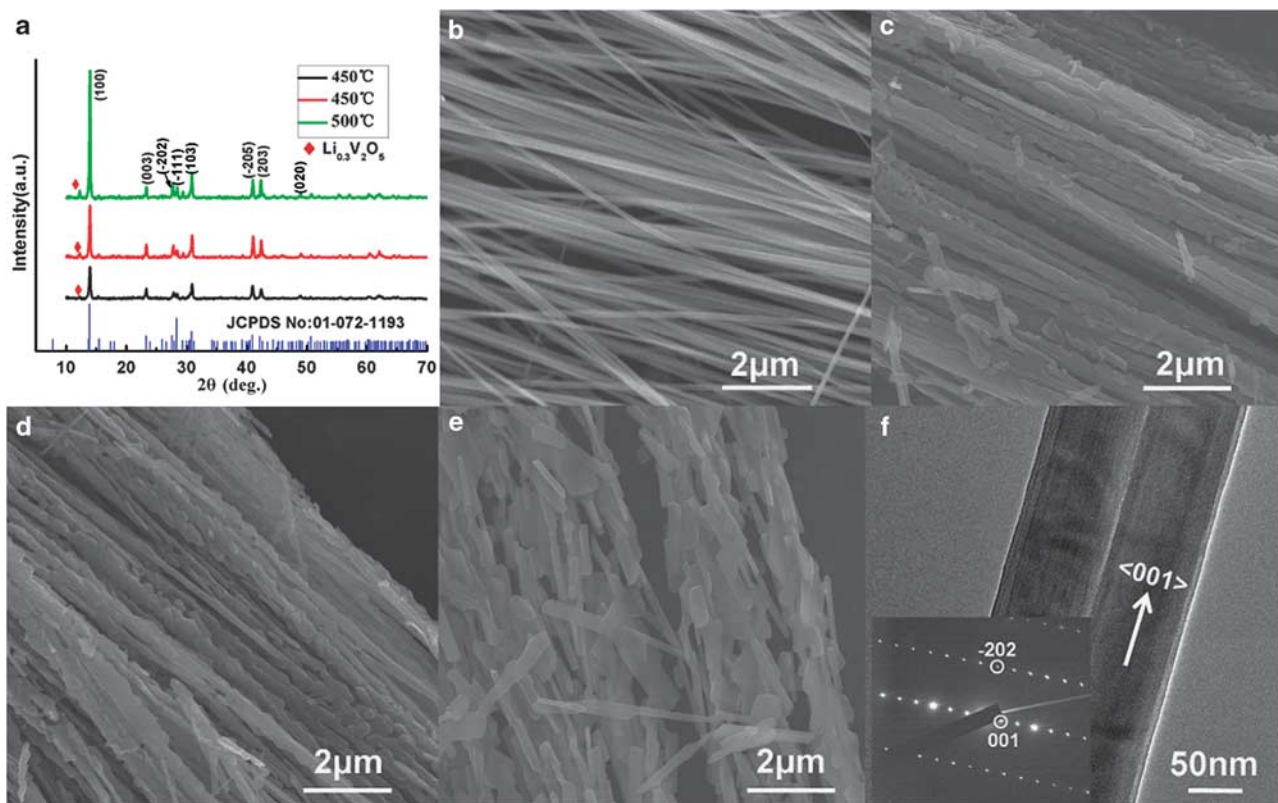


Figure 1 Phase, morphology and structure characterization. (a) X-ray diffraction patterns of LiV₃O₈ nanowires. (b–e) Scanning electron microscopy images of precursor H₂V₃O₈ nanowires and LiV₃O₈ nanowires at 400°C, 450°C and 500°C, respectively. (f) Transmission electron microscopy image and selected area electron diffraction pattern (inset) of LiV₃O₈ nanowires prepared at 450°C.

Table 1 Relative intensity ratios and BET surface area of LiV₃O₈ nanowires

Sample	I(100)	I(003)	I(020)	I(100)/I(003)	I(100)/I(020)	BET surface area
400 °C	1738	572	117	3.04	14.85	8.25 m ² g ⁻¹
450 °C	2795	706	156	3.96	17.92	9.99 m ² g ⁻¹
500 °C	6731	574	177	11.73	38.03	5.08 m ² g ⁻¹

Abbreviation: BET, Brunauer–Emmet–Teller.

material dissolution, passive film formation and loss of electrical contact.^{20,27,47} As the number of cycles increases, the passive film on the nanowire surface becomes stable, which would prevent further dissolution of the nanowire. At the same time, more active materials would participate in the electrochemical reaction, resulting first in an increase and then a stabilization of the capacity. This behavior became more noticeable during the following tests performed at higher current densities.

High-rate performance of LiV₃O₈ nanowire cathodes

In this work, ultralong LiV₃O₈ nanowires were designed to obtain a cathode material with a desirable high-rate performance. Sample 450 was found to have the best electrochemical performance, so it was chosen to investigate the high-rate performance. The battery was charged and discharged at different rates ranging from 50 to 1000 mA g⁻¹ (Figure 3a). The LiV₃O₈ nanowire cathode delivered the discharge capacities of 279, 269, 253, 237, 222, 211 and 196 mAh g⁻¹ at current densities of 50, 100, 200, 300, 400, 500

and 600 mA g⁻¹, respectively. Remarkably, even after 70 cycles, the capacity at the current density of 1000 mA g⁻¹ still reached 160 mAh g⁻¹. In addition, after this high-rate measurement, the battery with the LiV₃O₈ nanowire cathode was able to supply a high capacity of 269 mAh g⁻¹ at 50 mA g⁻¹. This performance indicates the excellent structural stability and the resulting high reversibility of LiV₃O₈ nanowires.

The high-rate capability of the LiV₃O₈ nanowire cathode was further studied (Figure 3b). Both of the specific discharge capacities decreased suddenly during the initial stage and then increased. The initial specific discharge capacities were 176 and 137 mAh g⁻¹ at the current densities of 1500 and 2000 mA g⁻¹, respectively. After 400 cycles, the capacity at 1500 mA g⁻¹ decreased to 160 mAh g⁻¹, corresponding to a capacity fading of 0.025% per cycle. After 600 cycles, the capacity at 2000 mA g⁻¹ decreased to 120 mAh g⁻¹, corresponding to a capacity fading of 0.022% per cycle. Meanwhile, the coulombic efficiencies both stayed at ~100% in the overall battery operation, indicating good reversibility.

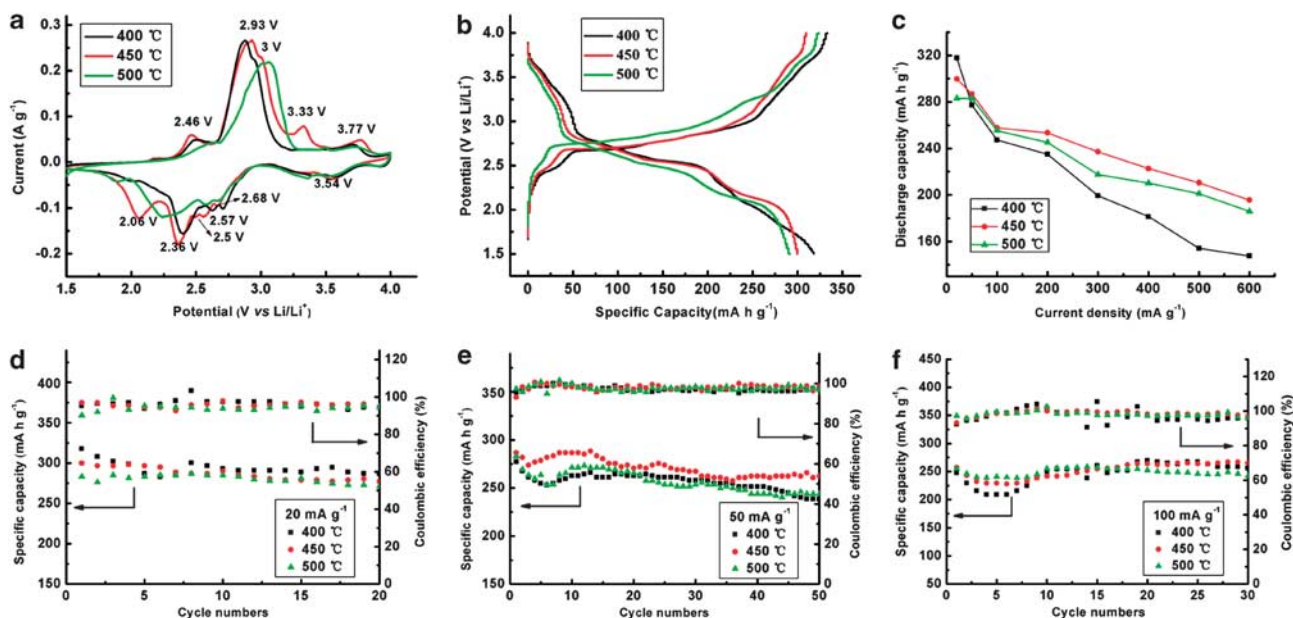


Figure 2 Electrochemical properties of LiV₃O₈ nanowires prepared at different calcination temperatures. (a) Cyclic voltammograms at a sweep rate of 0.1 mV s⁻¹ in the potential range from 4.0 to 1.5 V vs Li/Li⁺. (b) The initial charge–discharge curves at the current density of 20 mA g⁻¹. (c) The initial discharge capacities at different current densities. (d–f) The cycling performance at the current densities of 20, 50 and 100 mA g⁻¹, respectively.

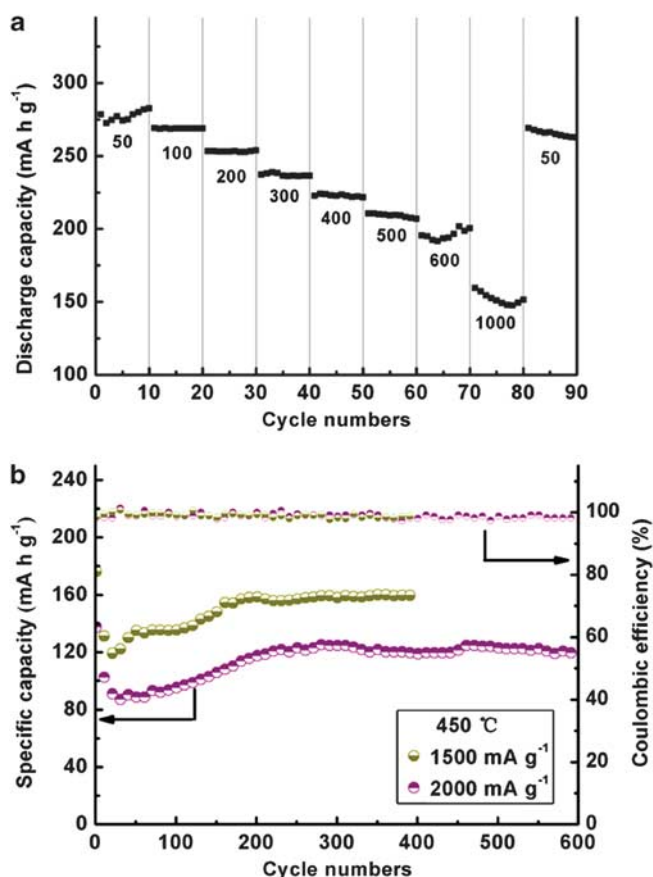


Figure 3 High-rate performance of the LiV₃O₈ nanowire cathode. (a) Discharge capacities of the LiV₃O₈ nanowire cathode at various current densities from 50 to 1000 mA g⁻¹. (b) Charge–discharge cycling test of the LiV₃O₈ nanowire cathode at high current densities of 1500 and 2000 mA g⁻¹.

LiV₃O₈ cathode materials have been widely investigated in recent years. Liu *et al.*²³ prepared LiV₃O₈ single-crystal nanorods by using a hydrothermal method combined with a solid-state method, which presented a high-specific discharge capacity of 236 mA h g⁻¹ at a current density of 100 mA g⁻¹ after 100 cycles. LiV₃O₈ nanomaterials have also been prepared by freeze-drying combined with an argon-atmosphere post-treated method, and the resulting nanomaterials exhibited a very high insertion capacity of 347 mA h g⁻¹ at a current density of 50 mA g⁻¹. Even after 60 cycles, a discharge capacity of 351 mA h g⁻¹ was obtained.²⁷ In spite of its remarkable capacity, the high-rate performance has rarely been studied. The highest reported current density was 1000 mA g⁻¹, and the LiV₃O₈ cathode showed a capacity of 158 mA h g⁻¹ after 100 cycles, with 0.23% capacity fading per cycle.¹⁹ A similar result was also obtained at this current density.³⁶ Compared with the reported LiV₃O₈ cathodes, the as prepared ultralong LiV₃O₈ nanowire cathode demonstrates a better high-rate performance. Moreover, the 400 cycles at 1500 mA g⁻¹ and 600 cycles at 2000 mA g⁻¹ with minimal capacity loss that were achieved with the LiV₃O₈ nanowire cathode indicate the very long life of the batteries. Such performance is comparable to other layered metal-oxide materials and indicates that the LiV₃O₈ nanowire cathode is a promising candidate for use in high-rate and long-life rechargeable Li batteries.^{48–51}

DISCUSSION

Calcination temperature has a significant impact on the nanowire size and space between the nanowires, which were reported to greatly influence the electrochemical performance of this material, especially for the high-rate charge/discharge process.^{19,20} It was found that 450 °C is the best calcination temperature, which may result from the fact that this temperature produces the most suitable degree of crystallinity and the resulting highest surface area (Table 1). A low degree of crystallinity of the electrode material is good for the capacity, and a high degree of crystallinity is good for the structural stability and the cycling performance, so identifying the most suitable

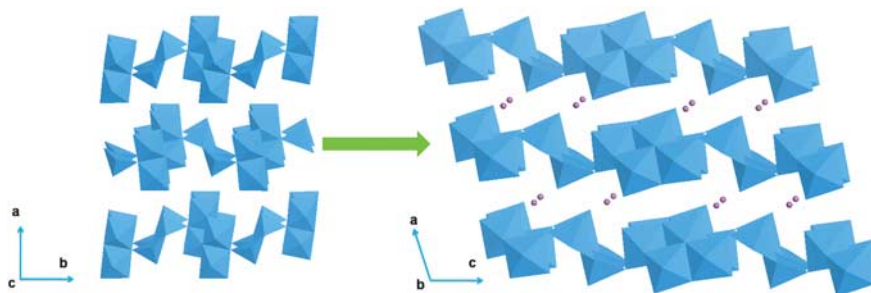
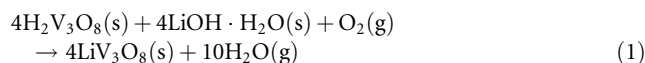


Figure 4 Crystal structure transformation from H₂V₃O₈ to LiV₃O₈.

degree of crystallinity is important for maximizing the overall performance of the electrode materials. A large electrode surface area can lead to a large electrode–electrolyte contact area, which will improve the high-rate performance. For sample 400, the nanowires had a low degree of crystallinity, and they aggregated. The space between the nanowires was limited, and the Brunauer–Emmet–Teller surface area was 8.25 m² g⁻¹. For sample 450, the crystal reorganization (according to the lowest-energy principle) was the dominant process causing the product to be in a more stable state. During this process, the volume decreased, leading to a larger space between the nanowires and a higher Brunauer–Emmet–Teller surface area of 9.99 m² g⁻¹, which was the highest for the three samples and also higher than the Brunauer–Emmet–Teller surface areas of all the reported LiV₃O₈ cathode materials.^{16,23,27} When the calcination temperature increased to 500 °C, nanowire crack/growth became the dominant process, and the crystallinity increased substantially, which resulted in a lower surface area of 5.08 m² g⁻¹. This conclusion can be confirmed by the XRD analysis and the calculated crystallinity result, indicating that the crystallinity increased only slightly from 400 to 450 °C but increased dramatically from 450 to 500 °C.

The precursor has a significant impact on the morphology, structure and electrochemical performance of the resultant nanomaterial. V₂O₅ nanowires have previously been used as a precursor to synthesize LiV₃O₈ nanomaterial.⁵² However, the uniform nanowire morphology of V₂O₅ was destroyed because there was a significant crystal structure change between the precursor V₂O₅ and the resultant LiV₃O₈. The concept of a topotactic intercalation mechanism was suggested to describe the formation of the Li₇MnP₄ phase from the MnP₄ phase through the insertion of Li ions,⁵³ which means that there are definite crystallographic relationships between the reactant and the product. Thus, we can obtain a product with a minimal change in structure and morphology from the reactant.^{54–56} In this work, the structure of the LiV₃O₈ product is made up of V₃O₈ layers consisting of VO₆ octahedra and VO₅ distorted trigonal bipyramids interconnected with each other.¹⁶ To realize the topotactic synthesis of LiV₃O₈ nanowires with a desirable high-rate performance, H₂V₃O₈ nanowires were chosen as the precursor. The nanowire structure also contains a layer structure composed of V₃O₈ layers consisting of VO₆ octahedra (V(1)O₆ and V(2)O₆) and VO₅ trigonal bipyramids (V(3)O₅) in which V(3) was assigned to V⁵⁺ and V(2) was likely V⁴⁺.³⁷ The crystal structures of LiV₃O₈ and H₂V₃O₈ are shown in Figure 4. The arrangements of VO polyhedra are similar, and the V₃O₈ layers are separated and stack along the a-axis in both structures. During the reaction with LiOH·H₂O, the Li ions can topotactically insert into the octahedral sites of H₂V₃O₈ without significantly changing the crystal structure. This may be the reason why LiV₃O₈ can generally maintain the nanowire morphology of H₂V₃O₈.

The reaction process between H₂V₃O₈ and LiOH·H₂O is presumed to occur as follows: after stirring in alcohol, H₂V₃O₈ and LiOH·H₂O close contact with each other. LiOH·H₂O has a lower melting point, so it acts as a diffusion medium and spreads over the surface of the H₂V₃O₈ nanowires as a result of Brownian motion. Because of the existence of the concentration gradient and the principle of minimum energy, Li ions diffuse into the H₂V₃O₈ nanowires and occupy the octahedral sites. Meanwhile, the V⁴⁺ in V(2) is oxidized to V⁵⁺ via the reaction with oxygen. The reaction equation is as follows:



Although both materials have similar layered structures, the presence of settled Li ions in the layers of the LiV₃O₈ structure has a significant impact on the structural stability during the charge–discharge process, which gives it a better electrochemical performance than H₂V₃O₈ (Supplementary Figure S3). At the current density of 100 mA g⁻¹, the initial discharge capacities were almost the same. However, after 30 cycles, the discharge capacity of LiV₃O₈ nanowires reached 265 mAh g⁻¹, whereas the capacity of H₂V₃O₈ nanowires was only 188 mAh g⁻¹. As the current density increasing to 500 mA g⁻¹, the initial discharge capacities were 201 and 151 mAh g⁻¹, respectively. After 200 cycles, the capacity of the LiV₃O₈ nanowire cathode was still 173 mAh g⁻¹, but the capacity of H₂V₃O₈ nanowires was only 146 mAh g⁻¹. The better battery performance of LiV₃O₈ nanowires can be attributed to two factors. First, in LiV₃O₈, Li ions occupy the octahedral sites and form ionic bonds with the V₃O₈ layers, which make the layered structure to be more stable than H₂V₃O₈ during the charge/discharge process. Second, LiV₃O₈ has lower charge transfer resistance than H₂V₃O₈, which is proved by the electrochemical impedance spectrometry test and the simulation results (Supplementary Figure S4). The charge transfer resistance (*R*_{ct}) of LiV₃O₈ is 218 Ω, much lower than the value of 597 Ω for H₂V₃O₈, which may be caused by the presence of Li ions in the LiV₃O₈ structure.

CONCLUSIONS

In summary, ultralong LiV₃O₈ nanowires have been synthesized by topotactic Li intercalation in H₂V₃O₈ nanowires. The LiV₃O₈ nanowire cathode showed excellent high-rate performance. A specific discharge capacity of 137 mAh g⁻¹ can be obtained at a current density of 2000 mA g⁻¹, and the capacity is able to stabilize at 120 mAh g⁻¹ even after 600 cycles, corresponding to 0.022% capacity fading per cycle. The excellent performance can be attributed to the low-charge-transfer resistance, good structural stability, large surface area and suitable degree of crystallinity. The good electrochemical performance of the ultralong LiV₃O₈ nanowire cathode indicates its

potential application in high-rate and long-life rechargeable Li batteries.

ACKNOWLEDGEMENTS

This work was supported by the National Natural Science Foundation of China (51072153), the Program for New Century Excellent Talents in University (NCET-10-0661), the National Basic Research Program of China (2012CB933003) and the Fundamental Research Funds for the Central Universities (2011-II-012, 2012-yb-02). We are grateful to Professor J Liu of the Pacific Northwest National Laboratory, Professor CM Lieber of Harvard University, Professor DY Zhao of Fudan University and Professor ZL Wang of Georgia Institute of Technology for their strong support and stimulating discussions. Thanks to Professor XD Bai and Ms LF Wang of the Institute of Physics (CAS, China), Professor JL Xie and Dr XQ Liu of the Center for Materials Research and Analysis of Wuhan University of Technology for materials characterization.

Author contributions: Xu Xu and Yanzhu Luo performed the experiments. Liqiang Mai, Xu Xu, Yanzhu Luo and Yunlong Zhao designed the experiments, discussed the interpretation of the results and co-wrote the paper. All authors discussed the results and commented on the manuscript.

- Kang, B. & Ceder, G. Battery materials for ultrafast charging and discharging. *Nature* **458**, 190–193 (2009).
- Tarascon, J. M. & Armand, M. Issues and challenges facing rechargeable lithium batteries. *Nature* **414**, 359–367 (2001).
- Liu, C., Li, F., Ma, L. P. & Cheng, H. M. Advanced materials for energy storage. *Adv. Mater.* **22**, E28–E62 (2010).
- Wu, Z. S., Ren, W. C., Xu, L., Li, F. & Cheng, H. M. Doped graphene sheets as anode materials with superhigh rate and large capacity for lithium ion batteries. *ACS Nano* **5**, 5463–5471 (2011).
- Tian, B. Z., Zheng, X. L., Kempa, T. J., Fang, Y., Yu, N. F., Yu, G. H., Huang, J. L. & Lieber, C. M. Coaxial silicon nanowires as solar cells and nanoelectronic power sources. *Nature* **449**, 885–890 (2007).
- Javey, A., Nam, S. W., Friedman, R. S., Yan, H. & Lieber, C. M. Layer-by-layer assembly of nanowires for three-dimensional, multifunctional electronics. *Nano Lett.* **7**, 773–777 (2007).
- Xu, S., Qin, Y., Xu, C., Wei, Y. G., Yang, R. S. & Wang, Z. L. Self-powered nanowire devices. *Nat. Nanotechnol.* **5**, 366–373 (2010).
- Lieber, C. M. & Wang, Z. L. Functional nanowires. *MRS Bull.* **32**, 99–108 (2007).
- Yan, H., Choe, H. S., Nam, S. W., Hu, Y. J., Das, S., Klemic, J. F., Ellenbogen, J. C. & Lieber, C. M. Programmable nanowire circuits for nanoprocessors. *Nature* **470**, 240–244 (2011).
- Mai, L. Q., Yang, F., Zhao, Y. L., Xu, X. & Luo, Y. Z. Hierarchical MnMo₄/CoMo₄ heterostructured nanowires with enhanced supercapacitor performance. *Nat. Commun.* **2**, 381 (2011).
- Chan, C. K., Peng, H. L., Twisten, R. D., Jarausch, K., Zhang, X. F. & Cui, Y. Fast, completely reversible Li insertion in vanadium pentoxide nanoribbons. *Nano Lett.* **7**, 490–495 (2007).
- Mai, L. Q., Xu, L., Han, C. H., Xu, X., Luo, Y. Z., Zhao, S. Y. & Zhao, Y. L. Electrospun ultralong hierarchical vanadium oxide nanowires with high performance for lithium ion batteries. *Nano Lett.* **10**, 4750–4755 (2010).
- Mai, L. Q., Hu, B., Chen, W., Qi, Y. Y., Lao, C. S., Yang, R. S., Dai, Y. & Wang, Z. L. Lithiated MoO₃ nanobelts with greatly improved performance for lithium batteries. *Adv. Mater.* **19**, 3712–3716 (2007).
- Liu, J. P., Jiang, J., Cheng, C. W., Li, H. X., Zhang, J. X., Gong, H. & Fan, H. J. Co₃O₄ nanowire @ MnO₂ ultrathin nanosheet core/shell arrays: A new class of high-performance pseudocapacitive materials. *Adv. Mater.* **23**, 2076–2081 (2011).
- Jiang, J., Liu, J. P., Zhou, W. W., Zhu, J. H., Huang, X. T., Qi, X. Y., Zhang, H. & Yu, T. CNTs/Ni hybrid nanostructured arrays: synthesis and application as high-performance electrode materials for pseudocapacitor. *Energy Environ. Sci.* **4**, 5000–5007 (2011).
- Sakunthala, A., Reddy, M. V., Chowdari, B. V. R. & Christopher, S. P. Preparation, characterization, and electrochemical performance of lithium trivanadate rods by a surfactant-assisted polymer precursor method for lithium batteries. *J. Phys. Chem. C* **114**, 8099–8107 (2010).
- Shi, Q., Ouyang, L. Z., Zeng, M. Q. & Zhu, M. High-capacity LiV₃O₈ thin-film cathode with a mixed amorphous–nanocrystalline microstructure prepared by RF magnetron sputtering. *Electrochim. Commun.* **11**, 2169–2172 (2009).
- Cui, C. J., Wu, G. M., Shen, J., Zhou, B., Zhang, Z. H., Yang, H. Y. & She, S. F. Synthesis and electrochemical performance of lithium vanadium oxide nanotubes as cathodes for rechargeable lithium-ion batteries. *Electrochim. Acta* **55**, 2536–2541 (2010).
- Pan, A. Q., Liu, J., Zhang, J. G., Cao, G. Z., Xu, W., Nie, Z. M., Jie, X., Choi, D. W., Arey, B. W., Wang, C. M. & Liang, S. Q. Template free synthesis of LiV₃O₈ nanorods as a cathode material for high-rate secondary lithium batteries. *J. Mater. Chem.* **21**, 1153–1161 (2011).
- Jouanneau, S., Verbaere, A., Lascaud, S. & Guyomard, D. Improvement of the lithium insertion properties of Li_{1-x}V₃O₈. *Solid State Ion.* **177**, 311–315 (2006).
- Liu, L., Jiao, L. F., Zhang, Y. H., Sun, J. L., Yang, L., Miao, Y. L., Yuan, H. T. & Wang, Y. M. Synthesis of LiV₃O₈ by an improved citric acid assisted sol-gel method at low temperature. *Mater. Chem. Phys.* **111**, 565–569 (2008).
- Liu, X. H., Wang, J. Q., Zhang, J. Y. & Yang, S. R. Sol-gel template synthesis of LiV₃O₈ nanowires. *J. Mater. Sci.* **42**, 867–871 (2007).
- Liu, H. M., Wang, Y. G., Wang, K. X., Wang, Y. R. & Zhou, H. S. Synthesis and electrochemical properties of single-crystalline LiV₃O₈ nanorods as cathode materials for rechargeable lithium batteries. *J. Power Sources* **192**, 668–673 (2009).
- Xu, H. Y., Wang, H., Song, Z. Q., Wang, Y. W., Yan, H. & Yoshimura, M. Novel chemical method for synthesis of LiV₃O₈ nanorods as cathode materials for lithium-ion batteries. *Electrochim. Acta* **49**, 349–353 (2004).
- Tran, N., Bramnik, K. G., Hibst, H., Pröll, J., Mronka, N., Holzapfel, M., Scheifele, W. & Novák, P. Spray-drying synthesis and electrochemical performance of lithium vanadates as positive electrode materials for lithium batteries. *J. Electrochem. Soc.* **155**, A384–A389 (2008).
- Brylev, O. A., Shlyakhtin, O. A., Egorov, A. V. & Tretyakov, Y. D. Phase formation and electrochemical properties of crychemically processed Li_{1+x}V₃O₈ materials. *J. Power Sources* **164**, 868–873 (2007).
- Liu, H. M., Wang, Y. G., Yang, W. S. & Zhou, H. S. A large capacity of LiV₃O₈ cathode material for rechargeable lithium-based batteries. *Electrochim. Acta* **56**, 1392–1398 (2011).
- Liu, Y. M., Zhou, X. C. & Guo, Y. L. Effects of reactant dispersion on the structure and electrochemical performance of Li_{1.2}V₃O₈. *J. Power Sources* **184**, 303–307 (2008).
- Kumagai, N. & Yu, A. S. Ultrasonically treated LiV₃O₈ as a cathode material for secondary lithium batteries. *J. Electrochem. Soc.* **144**, 830–835 (1997).
- Liu, Q. Y., Liu, H. W., Zhou, X. W., Cong, C. J. & Zhang, K. L. A soft chemistry synthesis and electrochemical properties of LiV₃O₈ as cathode material for lithium secondary batteries. *Solid State Ion.* **176**, 1549–1554 (2005).
- Patey, T. J., NG, S. H., Büchel, R., Tran, N., Krumeich, F., Wang, J., Liu, H. K. & Novak, P. Electrochemistry of LiV₃O₈ nanoparticles made by flame spray pyrolysis. *Electrochim. Solid-State Lett.* **11**, A46–A50 (2008).
- Xie, J. G., Li, J. X., Zhan, H. & Zhou, Y. H. Low-temperature sol-gel synthesis of Li_{1.2}V₃O₈ from V₂O₅ gel. *Mater. Lett.* **57**, 2682–2687 (2003).
- Wu, F., Wang, L., Wu, C., Bai, Y. & Wang, F. Study on Li_{1+x}V₃O₈ synthesized by microwave sol-gel route. *Mater. Chem. Phys.* **115**, 707–711 (2009).
- Yang, G., Wang, G. & Hou, W. H. Microwave solid-state synthesis of LiV₃O₈ as cathode material for lithium batteries. *J. Phys. Chem. B* **109**, 11186–11196 (2005).
- Zhou, Y., Yue, H. F., Zhang, X. Y. & Deng, X. Y. Preparation and characterization of LiV₃O₈ cathode material for lithium secondary batteries through an EDTA-sol-gel method. *Solid State Ionics* **179**, 1763–1767 (2008).
- Pan, A. Q., Zhang, J. G., Cao, G. Z., Liang, S. Q., Wang, C. M., Nie, Z. M., Arey, B. W., Xu, W., Liu, D. W., Xiao, J., Li, G. S. & Liu, J. Nanosheet-structured LiV₃O₈ with high capacity and excellent stability for high energy lithium batteries. *J. Mater. Chem.* **21**, 10077–10084 (2011).
- Oka, Y., Yao, T. & Yamamoto, N. Structure determination of H₂V₃O₈ by powder X-ray diffraction. *J. Solid State Chem.* **89**, 372–377 (1990).
- Mai, L. Q., Dong, Y. J., Xu, L. & Han, C. H. Single nanowire electrochemical devices. *Nano Lett.* **10**, 4273–4278 (2010).
- Liu, Y. M., Zhou, X. C. & Guo, Y. L. Effects of fluorine doping on the electrochemical properties of LiV₃O₈ cathode material. *Electrochim. Acta* **54**, 3184–3190 (2009).
- Zhang, H. L., Neilson, J. R. & Morse, D. E. Vapor-diffusion-controlled sol-gel synthesis of flaky lithium vanadium oxide and its electrochemical behavior. *J. Phys. Chem. C* **114**, 19550–19555 (2010).
- Liu, Y. M., Zhou, X. C. & Guo, Y. L. Structure and electrochemical performance of LiV₃O₈ synthesized by solid-state routine with quenching in freezing atmosphere. *Mater. Chem. Phys.* **114**, 915–919 (2009).
- Kawakita, J., Kato, T., Katayama, Y., Miura, T. & Kishi, T. Lithium insertion behaviour of Li_{1+x}V₃O₈ with different degrees of crystallinity. *J. Power Sources* **81–82**, 448–453 (1999).
- Ju, S. H. & Kang, Y. C. Effect of preparation temperature on the morphology, crystal structure and electrochemical properties of LiV₃O₈ powders prepared by spray pyrolysis. *Mater. Chem. Phys.* **126**, 133–137 (2011).
- Mai, L. Q., Xu, X., Han, C. H., Luo, Y. Z., Xu, L., Wu, Y. M. & Zhao, Y. L. Rational synthesis of silver vanadium oxides/polyaniline triaxial nanowires with enhanced electrochemical property. *Nano Lett.* **11**, 4992–4996 (2011).
- Kawakita, J., Miura, T. & Kishi, T. Lithium insertion into Li₄V₃O₈. *Solid State Ionics* **120**, 109–116 (1999).
- Kawakita, J., Katayama, Y., Miura, T. & Kishi, T. Structural properties of Li_{1+x}V₃O₈ upon lithium insertion at ambient and high temperature. *Solid State Ionics* **107**, 145–152 (1998).
- Tanguy, F., Gaubicher, J. & Guyomard, D. Capacity fading on cycling nano size grains of Li_{1.1}V₃O₈, electrochemical investigation. *Electrochim. Acta* **55**, 3979–3986 (2010).
- Liu, H. M. & Yang, W. S. Ultralong single crystalline V₂O₅ nanowire/graphene composite fabricated by a facile green approach and its lithium storage behavior. *Energy Environ. Sci.* **4**, 4000–4008 (2011).
- Yoo, H. C., Jo, M. K., Jin, B. S., Kim, H. S. & Cho, J. Flexible morphology design of 3D-macroporous LiMnPO₄ cathode materials for Li secondary batteries: ball to flake. *Adv. Energy Mater.* **1**, 347–351 (2011).
- Jeong, S. K., Park, S. J. & Cho, J. High-performance, layered, 3D-LiCoO₂ cathodes with a nanoscale Co₃O₄ coating via chemical etching. *Adv. Energy Mater.* **1**, 368–372 (2011).

- 51 von Bülow, J. F., Zhang, H. L. & Morse, D. E. Hydrothermal Realization of High-Power Nanocomposite Cathodes for Lithium Ion Batteries. *Adv. Energy Mater.* **2**, 309–315 (2012).
- 52 Zhao, P., Wang, D. S., Lu, J., Nan, C. Y., Xiao, X. L. & Li, Y. D. Synthesis of LiV₃O₈ nanorods and shape-dependent electrochemical performance. *J. Mater. Res.* **26**, 424–429 (2011).
- 53 Souza, D. C. S., Pralong, V., Jacobson, A. J. & Nazar, L. F. A reversible solid state crystalline transformation in a metal phosphide induced by redox chemistry. *Science* **296**, 2012–2015 (2002).
- 54 Ji, X. L., Lee, K. T. & Nazar, L. F. A highly ordered nanostructured carbon-sulphur cathode for lithium-sulphur batteries. *Nat. Mater.* **8**, 500–506 (2009).
- 55 Park, C. M., Kim, Y. U. & Sohn, H. J. Topotactic Li insertion/extraction in hexagonal vanadium monophosphide. *Chem. Mater.* **21**, 5566–5568 (2009).
- 56 Wen, P. H., Ishikawa, Y., Itoh, H. & Feng, Q. Topotactic transformation reaction from layered titanate nanosheets into anatase nanocrystals. *J. Phys. Chem. C* **113**, 20275–20280 (2009).



This work is licensed under the Creative Commons Attribution-NonCommercial-No Derivative Works 3.0 Unported License. To view a copy of this license, visit <http://creativecommons.org/licenses/by-nc-nd/3.0/>

Supplementary Information accompanies the paper on the NPG Asia Materials website (<http://www.nature.com/am>)